Zigzag ladders with staggered magnetic chirality in the $S=\frac{3}{2}$ compound β-$CaCr_2O_4$

Françoise Damay,[1,*] Christine Martin,[2] Vincent Hardy,[2] Antoine Maignan,[2] Gilles André,[1] Kevin Knight,[3] Sean R. Giblin,[3] and Laurent C. Chapon[3]

[1]*Laboratoire Léon Brillouin, CEA, CNRS UMR 12, 91191 Gif-Sur-Yvette Cedex, France*

[2]*Laboratoire CRISMAT, CNRS UMR 6508, 6 bvd Maréchal Juin, 14050 Caen Cedex, France*

[3]*ISIS Facility, Rutherford Appleton Laboratory-CCLRC, Chilton, Didcot, Oxfordshire OX11 0QX, United Kingdom*

(Received 12 June 2009; revised manuscript received 6 October 2009; published 7 June 2010)

The crystal and magnetic structures of the $S=\frac{3}{2}$ antiferromagnet β-$CaCr_2O_4$ have been investigated by means of specific heat, magnetization, muon relaxation, and neutron powder diffraction between 300 and 1.5 K. In this compound, in which the unusual topology of the Cr^{3+} magnetic lattice can be described as a network of triangular "zigzag" ladders with legs parallel to c, a complex antiferromagnetic ordering with an incommensurate propagation vector $\mathbf{k}=(0,0,q)$ ($q\sim0.477$ at 1.5 K) is evidenced below $T_N=21$ K. This complex magnetic ordering can be described as a honeycomblike arrangement of cycloids, running along c, and presenting a unique pattern of staggered chirality. To understand the experimental observation of this staggered chirality, we propose to use antisymmetric Dzyaloshinskii-Moriya terms in the exchange Hamiltonian.

DOI: 10.1103/PhysRevB.81.214405 PACS number(s): 75.25.−j, 75.10.Pq

I. INTRODUCTION

Geometrically frustrated antiferromagnetic materials have attracted considerable interest in condensed matter physics over the past few years, as frustration bears interesting consequences on spin structures, leading for example in the case of XXY or XYZ Heisenberg spins to exotic noncollinear magnetic ground states, as a way to release frustration through spontaneous symmetry breaking.[1,2] The most intensely studied examples of magnetic systems with geometric frustration are triangle-based lattices such as the stacked triangular lattice,[3,4] the Kagome lattices,[5,6] and the networks of corner-sharing[7] or edge-sharing tetrahedra.[8] Isotypes of calcium-ferrite $CaFe_2O_4$ (Refs. 9 and 10) offer an unusual way to study the impact of competing interactions on a magnetic arrangement, as they exhibit an original geometrically frustrated lattice, based on a honeycomblike mesh of triangular (or zigzag) ladders of magnetic atoms, further described below. Such structures have been the focus of relatively few experimental studies,[11–13] one of the most recent ones dealing with the quasi-one-dimensional magnetic character of the $S=1$ compound CaV_2O_4, in which gapless excitations have been observed,[14,15] and which has been suggested as a potential candidate for the study of the chiral gapless phase.[16]

In the present paper, we report on the magnetic properties of the $S=\frac{3}{2}$ compound β-$CaCr_2O_4$. In the room-temperature (RT) orthorhombic structure of β-$CaCr_2O_4$ (Fig. 1), isotype with $CaFe_2O_4$, the Cr^{+3} ions occupy two distinct crystallographic positions [labeled Cr(1) and Cr(2) in the following],

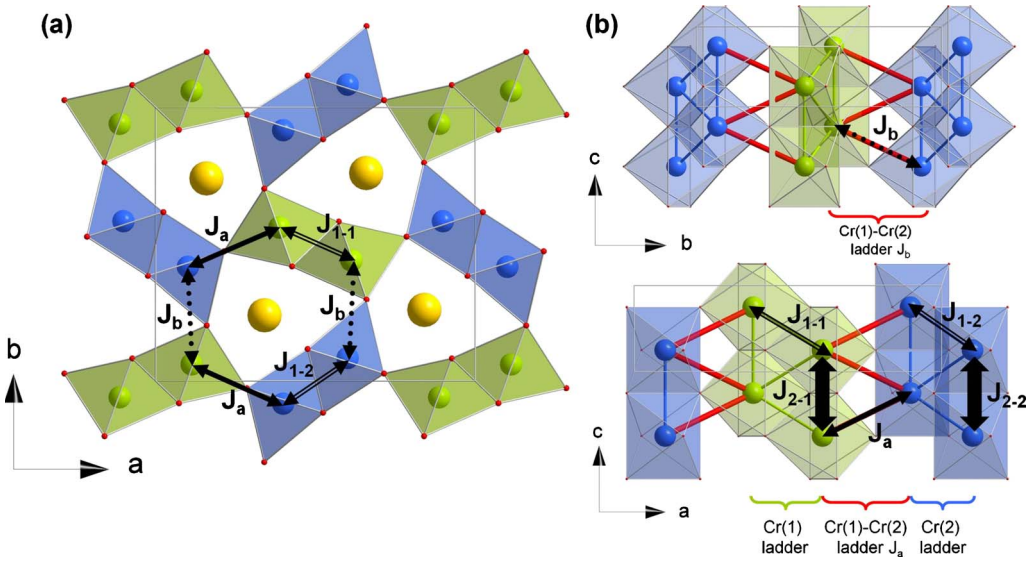

FIG. 1. (Color online) (a) Crystal structure of β-$CaCr_2O_4$ projected along [001], and (b) along [100] and [010]. The two distinct Cr^{3+} crystallographic sites Cr(1) and Cr(2), octahedrally coordinated by oxygen atoms, are shown as green and dark blue polyhedra, respectively. The different magnetic exchanges paths are shown by arrows (see text for details). The thick red bonds show the ladders rungs between adjacent chains on nonequivalent sites [Cr(1)/Cr(2)].

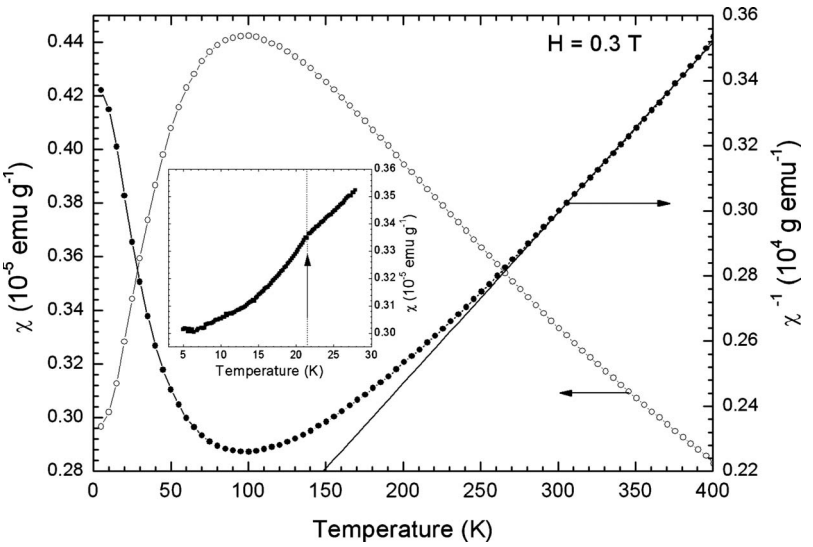

FIG. 2. Temperature evolution of the susceptibility and inverse susceptibility of β-$CaCr_2O_4$ in 0.3 T. Inset: ac susceptibility data of β-$CaCr_2O_4$ below $T=30$ K.

both on Wyckoff position $4c$ $(x,y,\frac{1}{4})$, and are octahedrally coordinated by oxygen ions. Symmetry equivalent CrO_6 octahedra form chains by sharing edges along the c axis [Fig. 1(b)]. The crystal symmetry is such that for any given chain in the lattice, the Cr positions in any adjacent chain irrespective of its nature are translated along c by (0, 0, 1/2) so that coupling between nearest chains either along the a axis or along the b axis has the so-called zigzag ladder topology [Fig. 1(b)]. The different chains are interconnected to create a honeycomblike network in the ab plane [Fig. 1(a)], the cavities of which host Ca^{2+} ions in prismatic coordination, slightly shifted from the center of their coordination prisms. According to this crystal-structure topology, antiferromagnetic nearest-neighbor coupling [$J_{2\text{-}1}$ and $J_{2\text{-}2}$ for the Cr(1) and Cr(2) chains respectively, see Fig. 1] is expected along the Cr chains, owing to the edge-sharing octahedral configuration allowing "cation-cation" direct exchange through the d_{xz} orbitals, which are pointing along the Cr-Cr axis. Next-nearest-neighbor interactions ($J_{1\text{-}1}$ and $J_{1\text{-}2}$) in ladders built with equivalent Cr atoms should also involve antiferromagnetic direct exchange. These ladders are interconnected through Cr-O-Cr bridges mediating a next-nearest-neighbor superexchange interaction (noted J_a and J_b depending on the direction of the Cr-O-Cr bridge).

Even though the crystal structure of β-$CaCr_2O_4$ was first reported 60 years ago,[17] to our knowledge, apart from an early study by Corliss *et al.*[18] mentioning a "complex" magnetic structure, the magnetic properties of this compound had not been investigated up to now and its magnetic structure is still unknown. Our study shows that below $T_N=21$ K, the long-range magnetic order observed in β-$CaCr_2O_4$ corresponds to a stacking of long-wavelength elliptical cycloidal modulations along c, presenting a unique pattern of staggered chiralities, based on zigzag ladders with either same or opposite leg chiralities. This observation cannot be interpreted in the framework of purely isotropic magnetic exchange but may be understood if one takes into account staggered Dzyaloshinkii-Moriya anisotropic exchange terms perpendicular to the ladder's legs.

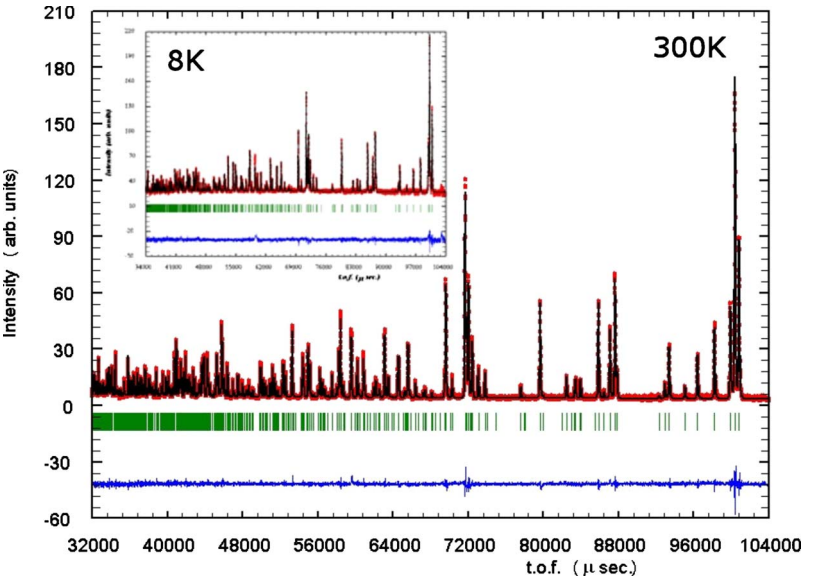

FIG. 3. (Color online) Rietveld refinement of time-of-flight neutron-diffraction data recorded on HRPD (ISIS) of β-$CaCr_2O_4$ at 300 K and (inset) 8 K (experimental data: open circles, calculated profile: continuous line, allowed Bragg reflections: vertical marks. The difference between the experimental and calculated profiles is displayed at the bottom of each graph).

TABLE I. Structural parameters of β-$CaCr_2O_4$ at 300, 100, and 8 K (from refinements of HRPD data). The space group is *Pbnm* and all the atoms are in site $4c$ $(x, y, \frac{1}{4})$.

		300 K	100 K	8 K
	a (Å)	10.6203(3)	10.6180(6)	10.6218(7)
	b (Å)	9.0801(3)	9.0737(6)	9.0763(6)
	c (Å)	2.9681(1)	2.9612(2)	2.9573(2)
	V (Å^3)	286.22(2)	285.29(3)	285.11(3)
Ca	x	0.6590(2)	0.6593(1)	0.6593(1)
	y	0.7598(2)	0.7601(2)	0.7604(2)
	B (Å^2)	0.44(3)	0.38(3)	0.32(3)
Cr(1)	x	0.6126(2)	0.6125(2)	0.6128(2)
	y	0.4398(2)	0.4394(2)	0.4397(2)
	B (Å^2)	0.29(3)	0.23(3)	0.17(3)
Cr(2)	x	0.1009(2)	0.1012(2)	0.1008(2)
	y	0.4165(2)	0.4159(2)	0.4161(2)
	B (Å^2)	0.27(2)	0.34(3)	0.31(5)
O(1)	x	0.1599(1)	0.1601(1)	0.1603(1)
	y	0.2026(1)	0.2026(1)	0.2027(1)
	B (Å^2)	0.34(2)	0.36(2)	0.35(2)
O(2)	x	0.4758(1)	0.4753(1)	0.4755(1)
	y	0.1165(1)	0.1170(1)	0.1173(1)
	B (Å^2)	0.29(2)	0.23(2)	0.25(2)
O(3)	x	0.7853(1)	0.7848(1)	0.7849(1)
	y	0.5267(1)	0.5263(1)	0.5263(1)
	B (Å^2)	0.33(2)	0.24(2)	0.24(2)
O(4)	x	0.4270(1)	0.4273(1)	0.4272(1)
	y	0.4180(1)	0.4172(2)	0.4172(2)
	B (Å^2)	0.31(2)	0.36(2)	0.29(3)
	R_{Bragg} (%)	3.20	3.42	3.57
	χ^2	2.47	4.45	4.84

II. EXPERIMENTAL

2 g of $CaCr_2O_4$ were prepared by high temperature solid-state reaction. Powders of CaO and Cr_2O_3 were weighted in the (1:1) stoichiometric ratio and heated at 1000 °C in air for a day. The powder was then pressed in the shape of pellets and heated to 1400 °C for 12 h in air, with a subsequent annealing at 1000 °C for 12 h in a reducing gas flow (5% H_2 in Ar). The samples obtained following this procedure were checked by room temperature x-ray diffraction and found to be single phase and of good crystallinity with the expected $CaFe_2O_4$-type structure.

Magnetic susceptibility defined as $\chi = M/H$ was calculated from magnetization data measured in a magnetic field of 0.3 T, on warming from 1.5 to 400 K, after a zero-field cooling, using a Quantum Design superconducting quantum interference device magnetometer. ac susceptibility was recorded in a commercial device [Physical Properties Measurements System (PPMS), Quantum Design] in an ac driving field $H_{ac} = 10^{-3}$ T ($H_{dc} = 0$), using a frequency of 10^4 Hz. Heat-capacity measurements were also carried out in a PPMS device using a relaxation method with a 2τ fitting procedure.

TABLE II. Selected distances (Å) and angles (°) in β-$CaCr_2O_4$ at 300, 100, and 8 K.

	300 K	100 K	8 K
Cr-Cr along c ($J_{2\text{-}1}$,$J_{2\text{-}2}$)	2.9681(1)	2.9611(1)	2.9573(1)
Cr(1)-Cr(1) ($J_{1\text{-}1}$)	3.0192(11)	3.0189(19)	3.0209(19)
Cr(1)-O(4)-Cr(1)	98.28(4)	98.21(7)	98.26(7)
Cr(2)-Cr(2) ($J_{1\text{-}2}$)	3.0154(11)	3.0219(21)	3.0157(22)
Cr(2)-O(2)-Cr(2)	97.70(3)	97.69(7)	97.53(7)
Cr(1)-Cr(2) (J_a)	3.6287(11)	3.6272(20)	3.6263(21)
Cr(1)-O(3)-Cr(2)	131.53(4)	131.71(7)	131.78(8)
Cr(1)-Cr(2) (J_b)	3.5615(12)	3.5501(23)	3.5543(23)
Cr(1)-O(1)-Cr(2)	121.99(4)	121.88(7)	121.92(7)

Neutron powder diffraction versus temperature was performed on the G4.1 diffractometer ($\lambda = 2.425$ Å) from 1.5 to 300 K, and a high-resolution neutron diffractogram at 10 K was recorded on the diffractometer 3T2 ($\lambda = 1.225$ Å). Both diffractometers are located at the LLB (CEA-Saclay, France). High-resolution neutron powder diffractograms were also recorded at 300, 100, and 8 K on the time-of-flight diffractometer HRPD (ISIS, U.K.). Rietveld refinements and determination of the magnetic symmetry with representation analysis were performed with programs of the FULLPROF suite.[19] Muon spin relaxation (μSR) was performed at the ISIS facility on the EMU beamline in order to further characterize any magnetic ordering on a local length scale.

III. RESULTS AND DISCUSSION

Susceptibility χ and inverse susceptibility curves obtained from magnetization measurements of β-$CaCr_2O_4$ between 2 and 400 K are presented in Fig. 2. The available data range is somewhat narrow to get reliable quantitative fitting values of a Curie-Weiss dependence, but between 350 and 400 K, the paramagnetic moment of Cr^{+3} can be estimated to be $3.89(5)\mu_B$ (the spin-only expected value is 3.87 for $S = \frac{3}{2}$), and the Weiss temperature θ_{CW} to be -239 ± 5 K, thus indicating predominantly antiferromagnetic correlations. On cooling below 280 K, the inverse susceptibility deviates increasingly from the Curie-Weiss law, until a broad maximum is evidenced around 90–100 K on the $\chi(T)$ curve. This maximum is followed by a pronounced drop, indicating the onset of three-dimensional (3D) antiferromagnetic interactions. Néel order is detectable as a small kink on the ac susceptibility data at $T = 21$ K (inset of Fig. 2). The magnetic ordering thus occurs at a much lower temperature than θ_{CW}, which suggests magnetic frustration [the frustration parameter $f = |\theta_{CW}|/T_C \sim 11$ (Ref. 20)] or low dimensionality of the magnetic behavior.

The RT structure of β-$CaCr_2O_4$, refined from the HRPD data (Fig. 3) in the *Pbnm* space group with $a = 10.6203(3)$ Å, $b = 9.0801(3)$ Å, $c = 2.9681(1)$ Å is found to be in excellent agreement with previous reports using single crystal x-ray diffraction[21] (Tables I and II). Both Cr^{3+}

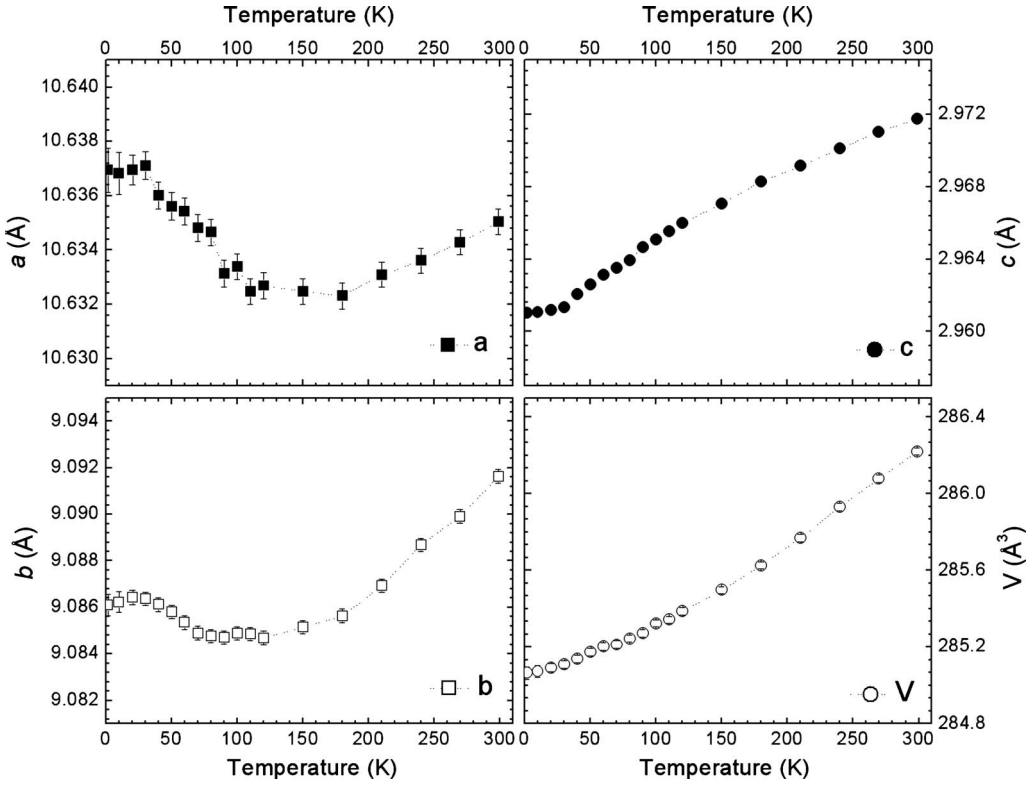

FIG. 4. Evolution with temperature of the β-$CaCr_2O_4$ cell parameters a, b, and c, and of cell volume V.

octahedra are weakly distorted with Cr-O distances ranging at 300 K between 1.9805(10) and 2.0410(11) Å, the $Cr(1)O_6$ octahedron being slightly more regular than the $Cr(2)O_6$ one. The average Cr-O distances in each Cr^{+3} octahedron are only marginally different, 2.0104(8) Å for $Cr(1)O_6$ and 2.0040(8) Å for $Cr(2)O_6$. Three out of the six bonds in each CrO_6 octahedron are involved in close to 98° angles between equivalent chromium sites while the three other bonds connect nonequivalent Cr sites together through Cr-O-Cr bridges close to 132° and 122° along a or b, respectively.

The HRPD neutron data recorded at 100 and 8 K (inset of Fig. 3) clearly show the absence of any modification of the crystal structure, which remains orthorhombic *Pbnm* down to 1.5 K (Table I). The evolution of the structural parameters as a function of temperature, extracted from Rietveld refinement of the G4.1 neutron data, indicates a clear anisotropic thermal cell contraction (Fig. 4). While the unit-cell volume follows a usual Debye function, a decreases with temperature until $T=100$ K and subsequently increases before becoming constant for $T<30$ K. A similar trend is observed for the b parameter but with lesser variations below 100 K. In contrast, c decreases steadily down to 30 K and levels out below. This anisotropic contraction of the cell corresponds to a substantial shortening of the Cr-Cr distance within the Cr chains running along c, simultaneously with a reduction in the Cr(1)-Cr(2) distance corresponding to the superexchange J_b (Table II). Rung distances between equivalent Cr sites do not vary significantly with temperature.

In agreement with the susceptibility data, above $T=21$ K (T_{N1}), a broad asymmetric feature, centered around the $(1,0,\frac{1}{2})$ Bragg position, is observed on the neutron diffraction data [Fig. 5(a) left and right]. This scattering becomes more diffuse and comparable to the background level on warming above 180 K. However, the susceptibility suggests that this effect should persist up to 280 K, temperature at which the deviation from the Curie-Weiss law becomes clearly noticeable. Between T_{N1} and T_{N2} [Figs. 5(a) and 5(b)], the diffuse scattering signal decreases and the first magnetic Bragg peaks appear, which can be indexed with a propagation vector $k=(0,0,q)$ $[q\sim0.479(1)]$ roughly constant within this temperature range. For $T<T_{N2}$, a strong decrease in q is observed, and a large fraction of the magnetic diffuse intensity is transferred into magnetic Bragg reflections, all indexed with the propagation vector $\mathbf{k}=(0,0,q)$ $[q\sim0.477(1)$ at 1.5 K]; at 1.5 K, the magnetic signal is mainly found in Bragg scattering [Fig. 5(a)] even though a persistent contribution from the weak diffuse signal is still observable.

A muon relaxation experiment [Fig. 5(d)] corroborates the long-range magnetic order at T_{N1}: fitting the relaxation spectra with an exponential of the form $A(t)=A_0\exp(-\lambda t)$, with A_0 the normalized amplitude of the asymmetry and λ the fluctuation rate, a clear drop in the asymmetry by 2/3, along with a slowing down of the dynamics—both indications of a long range magnetic transition in μSR—are evidenced at $T_{N1}\sim21$ K (a critical-type fit to the value of A_0 gives a magnetic ordering temperature of 21.6 K).

Additional heat capacity measurements also show that in this temperature range, two peaks are actually observed [Fig. 5(c)]: the first one, at $T_{N1}=21$ K, is associated with the onset of the 3D long-range antiferromagnetic ordering in agree-

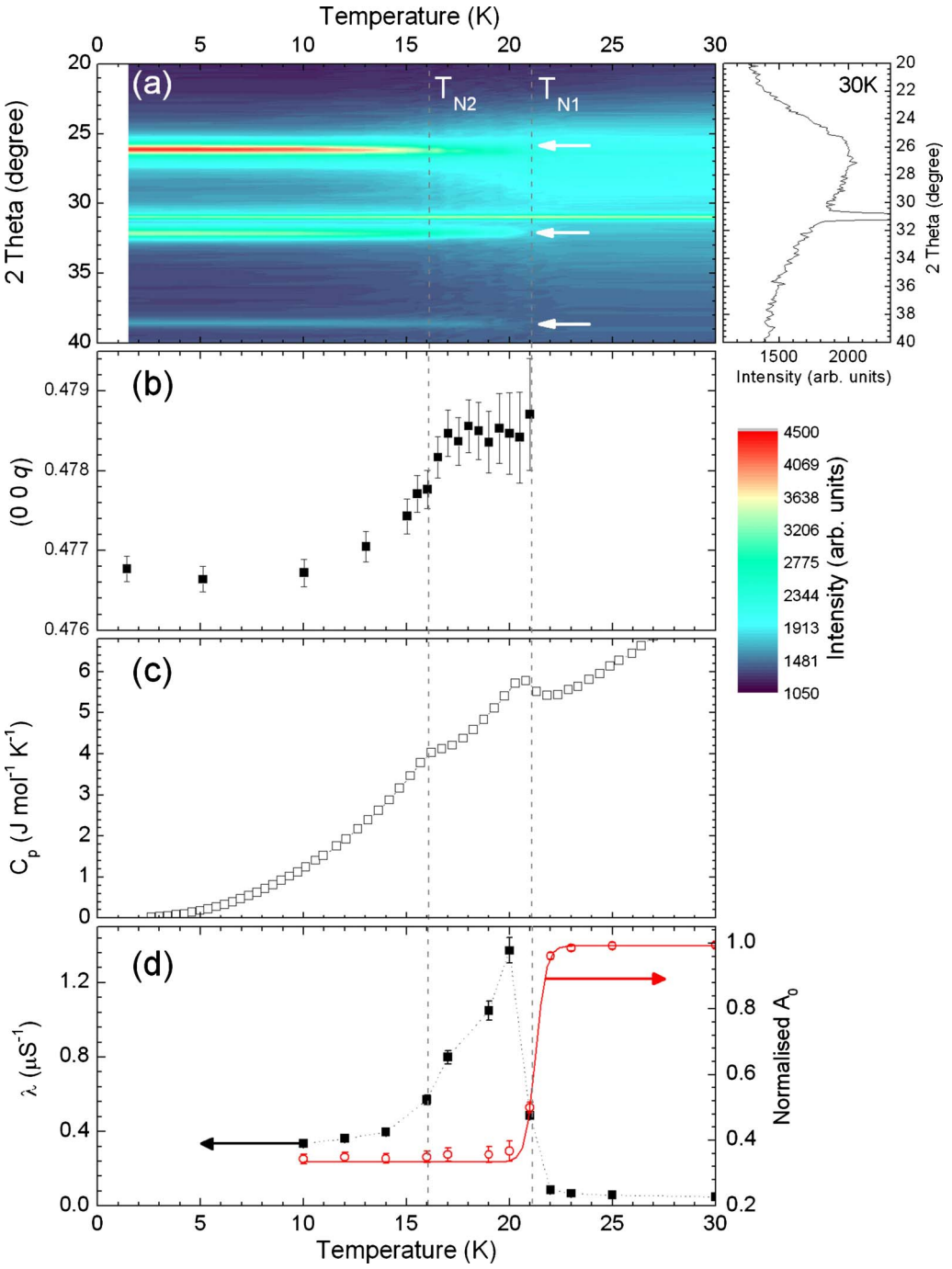

FIG. 5. (Color online) (a) Left: evolution with temperature of the neutron diffractograms (G4.1) of β-$CaCr_2O_4$. T_{N1} and T_{N2} refer to the transition temperatures observed on the specific-heat data. Arrows indicate magnetic Bragg peaks. Right: profile of the diffuse magnetic scattering at 30 K. (b) Temperature dependence of the q component of the magnetic propagation vector $k=(0,0,q)$. (c) Specific heat C_p versus temperature of β-$CaCr_2O_4$. (d) Temperature dependence of the normalized initial asymmetry (red circles) and fluctuation rate (λ, black solid squares) obtained from μSR. The solid line is a fit using a critical exponent to obtain an approximate ordering temperature.

ment with neutron diffraction, while the second one, T_{N2} =16 K, is attributed to another magnetic transition, as will be discussed below.

The low-temperature magnetic structure has been determined by Rietveld refinement using symmetry adapted modes derived from representation analysis.[19] There are four one-dimensional irreducible representations of the little group G_k. The magnetic representation Γ_m calculated for the Wyckoff position 4c in the *Pbnm* space group (for both Cr sites) contains three times each representation so that there are three basis functions for each representation. Only the symmetry modes spanned by the irreducible representation Γ_3 (following Kovalev notation[22]) provide good agreement with the experimental data. Table III lists the basis vectors of irreducible representation Γ_3, obtained by the projection operators method. An unconstrained refinement, using only the

TABLE III. Basis functions for axial vectors associated with irreducible representation Γ_3 for Wyckoff site 4*c*. $a=e^{+i\pi q}$.

Γ_3	(x,y,z) Cr(1)-1	$(-x+1,-y+1,z+\frac{1}{2})$ Cr(1)-2	$(-x+\frac{3}{2},y+\frac{1}{2},z)$ Cr(1)-3	$(x-\frac{1}{2},-y+\frac{1}{2},z+\frac{1}{2})$ Cr(1)-4
ψ_1	(1 0 0)	(a^* 0 0)	(−1 0 0)	(−a^* 0 0)
ψ_2	(0 1 0)	(0 a^* 0)	(0 1 0)	(0 a^* 0)
ψ_3	(0 0 1)	(0 0 −a^*)	(0 0 1)	(0 0 −a^*)

symmetry restrictions of Γ_3, shows that the components of the magnetic moments along the crystallographic axes are nearly equivalent for both Cr sites. As a result, in the final refinement stage, these components were constrained to be equal. There are two indistinguishable moment configurations, with identical magnetic structure factors, that give a very good agreement factor $R_{\text{mag}}=4.7\%$ [Fig. 6(a)] with the experimental data. They are illustrated on Fig. 6(b). The first model (i) consists of a sinusoidal modulation of the moment amplitude, and is obtained by mixing the basis functions ψ_1 and ψ_3 with real components. The second model (ii) describes a cycloidal elliptical modulation, obtained by mixing ψ_1 and ψ_3 with real and imaginary characters, $\psi=\psi_1+i\psi_3$. For both models, the magnetic moments lay in the *ac* plane. At 1.5 K, the components of the moment are $M_x=2.88(7)\mu_B$ and $M_z=1.27(13)\mu_B$ along the *a* and *c* directions, respectively. For model (i), this means that the wave maximum amplitude is about $3.14(8)\mu_B$, while for model (ii), the ordered component maximum is simply the major axis of the ellipse (M_x). While it is impossible to distinguish between both models by diffraction on a polycrystalline sample,[23] the moment value found for model (i), slightly exceeding the expected spin value of $3.0\mu_B$, is nonphysical. In addition, the existence of two transitions in the temperature dependence of the specific heat suggests that the cycloidal model is much more likely, and is actually reminiscent of the successive transitions seen in numerous magnetic systems presenting noncollinear complex magnetic orderings,[24,25] such as those with competing interactions in the presence of single ion anisotropy.[4] It is also a known feature of $S=\frac{1}{2}$ quantum spin chains compounds such as $LiCu_2O_2$ (Ref. 26) or $NaCu_2O_2$.[27] In these systems, although only a broad maximum, characteristic of short-range correlations within the chains, is evidenced on susceptibility curves, two peaks are observed on the specific-heat data and successive magnetic phase transitions have been confirmed by NMR measurements.[28,29] In this respect, the first transition can therefore be understood as a collinear spin-density wave with the moments oriented along the anisotropy direction (the *a* axis, which is the major axis of the elliptical modulation), while T_{N2} is indicative of the onset of a secondary order parameter along *c*, which increases the single-ion

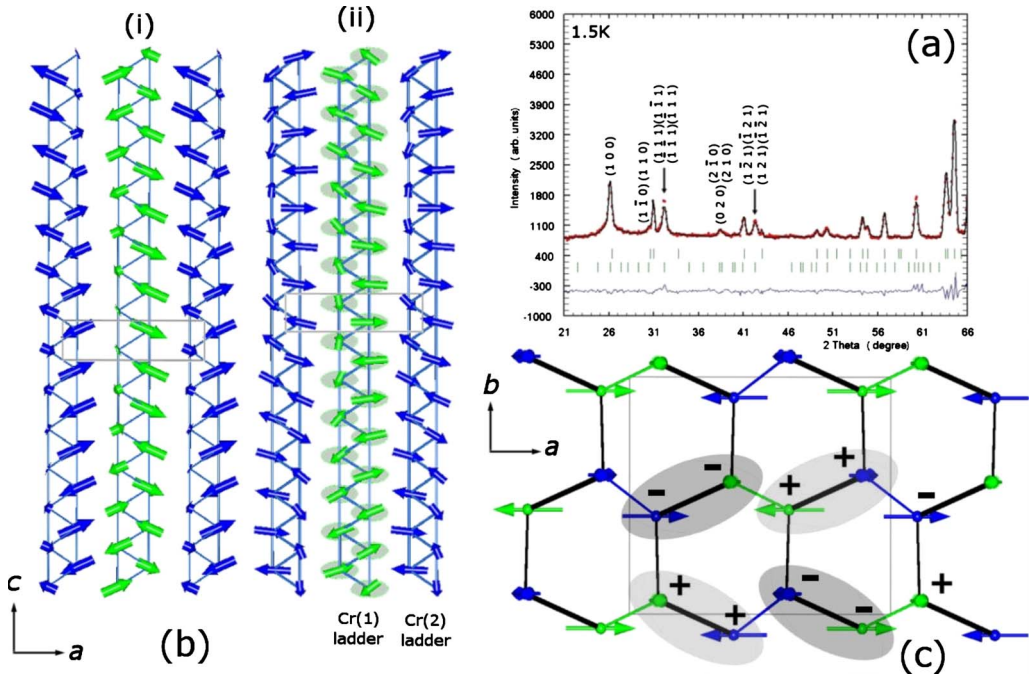

FIG. 6. (Color online) (a) Low angle enlargement of the Rietveld refinement of the neutron-diffraction data (G4.1) of β-$CaCr_2O_4$ at 1.5 K (experimental data: open circles, calculated profile: continuous line, allowed Bragg reflections: vertical marks. The difference between the experimental and calculated profiles is displayed at the bottom of each graph). (b) Sinusoidal (i) and cycloidal (ii) magnetic spin configurations along equivalent chromium ladders. (c) Distribution of the sign of the chirality along *c* within Cr chains in the honeycomb lattice. Same leg chirality ladders are outlined in gray.

anisotropy energy but lowers the magnetic entropy dominant at low temperature. The larger amplitude of the first peak in the heat capacity measurement, as well as the variation in the moment components with temperature (M_x/M_z=2.26 at 1.5 K and M_x/M_z=2.52 at 20 K) actually corroborate this assumption.

The magnetic point symmetry can be easily deduced from the analysis of the corepresentation analysis.[30] Since the experimental mode is a combination $\Delta_3+i\Delta_3$, all operations of the co-little group combined with complex conjugation are lost, and the point symmetry is *mm*2. This symmetry can support ferroelectricity along the *c* axis. In addition, in the $T<T_{N2}$ cycloidal magnetic arrangement of β-$CaCr_2O_4$, the basis functions for representation Γ_3 actually point out a nonuniform chirality of the cycloidal modulations along Cr chains parallel to *c* and involving Cr atoms on equivalent sites. Indeed, the sign of the imaginary *z* component of the basis function ψ_3 is opposite for Cr(1)-1 and Cr(1)-2, on one hand, and for Cr(1)-3 and Cr(1)-4, on the other hand, while the sign of the *x* component of ψ_1 is kept the same (Table III): as a result, ladders made of Cr(1)-1 and Cr(1)-2 legs have opposite leg chiralities, and so do ladders with Cr(1)-3 and Cr(1)-4 legs. In contrast, Cr(1)-1 and Cr(1)-4 chains [or Cr(1)-2 and Cr(1)-3 chains] have the same chirality. The same applies to Cr(2) atoms. The chirality pattern is therefore dictated by the symmetry relations, themselves imposed by the different magnetic coupling terms in competition. The only freedom is in the choice of coupling between Cr(1) and Cr(2), which is antiferromagnetic along *a* and ferromagnetic along *c* according to the refinement. Figure 6(c) shows the resulting chirality arrangement in the *ab* plane with symbols + and − labeling chains with opposite chiralities. It is noteworthy that only the chains with next-nearest-neighbor coupling J_a, also called J_a ladders, exhibit the same sign chirality. Same sign leg chirality in a zigzag ladder is indeed the expected configuration, at least in the classical limit, if one considers only isotropic exchange interactions.[31] As a result, to take into account the opposite chiralities observed within J_1 or J_b ladders, we propose to consider an additional anisotropic exchange term such as a Dzyaloshinskii-Moriya (DM) interaction perturbation, of the type $E_{DM}=D\cdot\mathbf{S}_i\times\mathbf{S}_j$ (*i* and *j* refer to first-neighbor ions along a chain). As relativistic corrections, these terms are usually small, but can become significant when competing with a weak isotropic exchange integral. Based on symmetry considerations illustrated on Fig. 7, the **D** vector would be directed in the *xy* plane and its *y* component would couple to noncollinear spin arrangements in the *xz* plane, as observed experimentally; its direction is reversed by the twofold rotation (screw axis) along the *z* axis that relates each legs of the Cr(1)-Cr(1) ladders and each legs of the Cr(2)-Cr(2) ladders, thus explaining the reversed chiralities. DM interactions between Cr(1)-Cr(1) sites and Cr(2)-Cr(2) sites along the rungs are not permitted since these atoms are related by an inversion point. For the J_b ladder, in which both legs also have opposite chiralities, since Cr(1) and Cr(2) are not related by any symmetry operations of the paramagnetic group, the **D** vector can point in a general direction, and must also play a role in determining the opposite chiralities of the ladder legs. In this picture, the staggered chirality pattern therefore results from a direct competition between the weak isotropic nearest-neighbor exchange interaction (such as $J_{1\text{-}1}$, $J_{1\text{-}2}$, or J_b), that favors uniform chirality between ladder legs and a staggered DM interaction along each ladder's leg, that favors opposite leg chiralities.

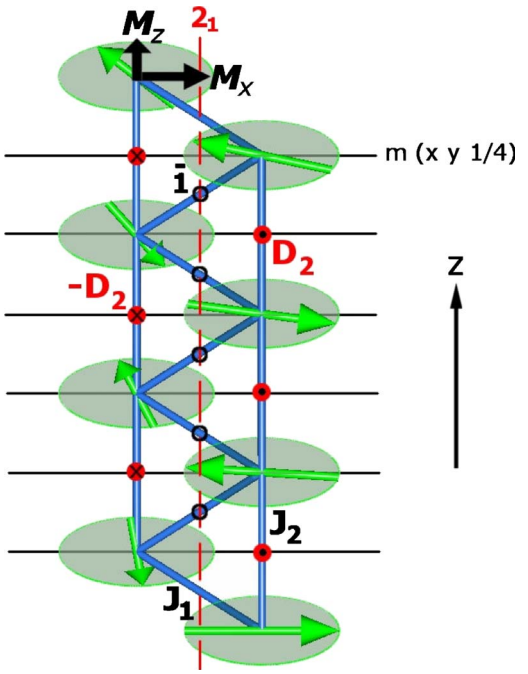

FIG. 7. (Color online) Schematic representation of a zigzag ladder between equivalent Cr atoms with its symmetry elements and of its magnetic cycloidal modulation (shown as elliptical envelops) in the *ac* plane (M_x and M_z). Chiralities are opposite between the two chains (atom 1 and atom 2). The isotropic exchange nearest and next-nearest interactions J_1 and J_2, as well as the antisymmetric DM vectors (D_2), are shown.

IV. CONCLUSION

The combination of susceptibility, heat capacity, muon relaxation, and neutron scattering measurements carried out on β-$CaCr_2O_4$, which exhibits a $S=\frac{3}{2}$ triangular ladder topology, allowed us to characterize the complex antiferromagnetic transition that is observed at $T=21$ K in this compound. The main originality of the cycloidal magnetic ordering evidenced lies in the nonuniform leg chiralities of the Cr^{+3} ladders, which suggests that the symmetric magnetic exchange interaction within the ladder's rungs is in direct competition with antisymmetric exchange terms along the ladders legs.

ACKNOWLEDGMENTS

Authors acknowledge fruitful discussions with S. Petit (LLB) and thank F. Porcher for the neutron diffraction data on 3T2 (LLB). Financial support for this work was partially provided by the French Agence Nationale de la Recherche, Grant No ANR-08-BLAN-0005-01.

*francoise.damay@cea.fr

[1] J. Villain, J. Phys. Chem. Solids **11**, 303 (1959).
[2] A. Yoshimori, J. Phys. Soc. Jpn. **14**, 807 (1959).
[3] H. Kawamura, J. Phys.: Condens. Matter **10**, 4707 (1998).
[4] M. F. Collins and O. A. Petrenko, Can. J. Phys. **75**, 605 (1997).
[5] A. P. Ramirez, G. P. Espinosa, and A. S. Cooper, Phys. Rev. Lett. **64**, 2070 (1990).
[6] P. Schiffer, A. P. Ramirez, D. A. Huse, and A. J. Valention, Phys. Rev. Lett. **73**, 2500 (1994).
[7] S. T. Bramwell and M. J. P. Gingras, Science **294**, 1495 (2001).
[8] K. Binder, Phys. Rev. Lett. **45**, 811 (1980).
[9] F. Bertaut, P. Blum, and G. Magnano, Acad. Sci., Paris, C. R. **241**, 757 (1955).
[10] P. M. Hill, H. S. Peiser, and J. R. Rait, Acta Crystallogr. **9**, 981 (1956).
[11] H. Karunadasa, Q. Huang, B. G. Ueland, J. W. Lynn, P. Schiffer, K. A. Regan, and R. J. Cava, Phys. Rev. B **71**, 144414 (2005).
[12] O. A. Petrenko, G. Balakrishnan, N. Wilson, S. de Brion, E. Suard, and L. Chapon, Phys. Rev. B **78**, 184410 (2008).
[13] A. Niazi, S. L. Bud'ko, D. L. Schlagel, J. Q. Yan, T. A. Lograsso, A. Kreyssig, S. Das, S. Nandi, A. I. Goldman, A. Honecker, R. W. McCallum, M. Reehuis, O. Pieper, B. Lake, and D. C. Johnston, Phys. Rev. B **79**, 104432 (2009).
[14] H. Kikuchi, M. Chiba, and T. Kubo, Can. J. Phys. **79**, 1551 (2001).
[15] H. Fukushima, H. Kikuchi, M. Chiba, Y. Fujii, Y. Yamamoto, and H. Hori, Prog. Theor. Phys. Suppl. **145**, 72 (2002).
[16] T. Hikihara, M. Kaburagi, and H. Kawamura, Phys. Rev. B **63**, 174430 (2001).
[17] W. Ford and W. J. Rees, Trans. Br. Ceram. Soc. **48**, 291 (1949).
[18] L. M. Corliss, J. M. Hastings, and W. Kunnmann, Phys. Rev. **160**, 408 (1967).
[19] J. Rodriguez-Carvajal, Physica B **192**, 55 (1993).
[20] A. P. Ramirez, *Handbook of Magnetic Materials* (Elsevier Science B. V., North Holland, 2001), Vol. 13, Chap. 4, pp. 423–521.
[21] W. Horkner and H. Müller-Buschbaum, Z. Naturforsch., B **31**, 1710 (1976).
[22] O. Kovalev, *Representations of the Crystallographic Space Groups* (Gordon and Breach, New York, 1993).
[23] Only neutron polarimetry on a single crystal would be able to distinguish between the two models.
[24] T. Kimura, T. Goto, H. Shintani, K. Ishizaka, T. Arima, and Y. Tokura, Nature (London) **426**, 55 (2003).
[25] A. H. Arkenbout, T. T. M. Palstra, T. Siegrist, and T. Kimura, Phys. Rev. B **74**, 184431 (2006).
[26] T. Masuda, A. Zheludev, A. Bush, M. Markina, and A. Vasiliev, Phys. Rev. Lett. **92**, 177201 (2004).
[27] L. Capogna, M. Mayr, P. Horsch, M. Raichle, R. K. Kremer, M. Sofin, A. Maljuk, M. Jansen, and B. Keimer, Phys. Rev. B **71**, 140402 (2005).
[28] A. A. Gippius, E. N. Morozova, A. S. Moskvin, A. V. Zalessky, A. A. Bush, M. Baenitz, H. Rosner, and S. L. Drechsler, Phys. Rev. B **70**, 020406 (2004).
[29] A. A. Gippius, A. S. Moskvin, and S. L. Drechsler, Phys. Rev. B **77**, 180403 (2008).
[30] P. G. Radaelli and L. C. Chapon, Phys. Rev. B **76**, 054428 (2007).
[31] J. Villain, J. Phys. **38**, 385 (1977).